PNAS
www.pnas.org

Supplementary Information for

A direct and widespread role for the nuclear receptor EcR in mediating the response to ecdysone in *Drosophila*

Christopher M. Uyehara and Daniel J. McKay

Daniel J. McKay
Email: dmckay1@email.unc.edu

This PDF file includes:

Supplementary text
Figs. S1 to S12
Tables S1 to S4
References for SI reference citations

Other supplementary materials for this manuscript include the following:
Datasets S1 to S5

www.pnas.org/cgi/doi/10.1073/pnas.1900343116

Supplementary Materials and Methods

Western Blots

For each sample, 40 wings were lysed directly in Laemmli sample buffer preheated to 95C. Samples were run on a BioRad 7.5% Mini-Protean TGX gel at 90V for 60m and then transferred to a nitrocellulose membrane at 100V for 60m. Membranes were blocked in 5% carnation instant milk for 30m at room temperature (RT) or overnight at 4C. Primary and secondary antibodies were incubated for 2hr at RT using four washes with 1XTBST between incubations. The following antibody concentrations were used to probe blots: 1:1000 mouse anti-EcR (DSHB DDA2.7, concentrate); 1:1000 anti-EcR-A (DSHB 15G1a, concentrate), 1:1000 anti-EcR-B1 (DSHB AD4.4, concentrate); 1:5000 rabbit anti-GFP (Abcam ab290); 1:30000 mouse anti-alpha Tubulin (Sigma T6074); 1:5000 goat anti-mouse IgG, HRP-conjugated (Fisher 31430); 1:5000 donkey anti-rabbit, HRP-conjugated (GE Healthcare NA934). Membranes were imaged on a GE Amersham Imager 600.

Transgenic Reporter Construction

Candidate enhancers were cloned into the pΦUGG destination vector (1) and integrated into the attP2 site. Primer sequences are available upon request.

Immunofluorescence

Immunostaining was performed as described previously (2). For mitotic clones, *usp3 FRT19A / Ubi-RFP, hs-FLP, FRT19A; Enhancer-GAL4 / UAS-dsGFP* animals were heat-shocked at 24-48hrs AEL. The following antibody concentrations were used: 1:750 mouse anti-EcR (DSHB DDA2.7, concentrate), 1:4000 rabbit anti-GFP (Abcam ab290), 1:3500 mouse anti-Dl (DSHB C594.9b, concentrate), 1:200 mouse anti-FLAG M2 (Sigma F1804), 1:10 mouse anti-Achaete (DSHB anti-Achaete, supernatant), 1:1000 anti-Br (DSHB 25E9.D7, concentrate). Samples were imaged on a Leica Sp5 confocal microscope.

Sample preparation for RNAseq

A minimum of 60 wings were prepared as previously described (2) from either *Oregon R* (WT) or *yw; vg-GAL4, Tub>>CD2>>GAL4, UAS-GFP, UAS-FLP / UAS-EcR-RNAi*^{104} (EcR-RNAi). For library construction, 50-100ng RNA was used as input to the Ovation *Drosophila* RNA-Seq System. Single-end, 1x50 sequencing was performed on an Illumina HiSeq 2500 at the UNC High Throughput Sequencing Facility.

Sample preparation for CUT&RUN

A minimum of 100 wings from *w; EcR*^{GFSTF}*/Df(2R)BSC889* were dissected in 1XPBS. Samples were centrifuged at 800g for 5 minutes at 4C and washed twice with dig-wash buffer (20mM HEPES-NaOH, 150mM NaCl, 2mM EDTA, 0.5mM Spermidine, 10mM PMSF, 0.05% digitonin) and incubated in primary antibody for 2hrs at 4C. Samples were washed as before and incubated in secondary antibody for 2hrs. Samples were washed as before and incubated for 1hr with protein-A MNase. Samples were washed twice in dig-wash buffer without EDTA and then resuspended in 150uL dig-wash buffer without EDTA. Following this, samples were equilibrated to 0C in an ice bath. 2uL $CaCl_2$ (100mM) was added to activate MNase and digestion allowed to proceed for 45s before treating with 150uL 2XRSTOP+ buffer (200mM NaCl, 20mM EDTA, 4mM EGTA, 50ug/ml RNase, 40ug/ml glycogen, 2pg/ml yeast spike-in DNA). Soluble fragments were released by incubating at 37C for 10m. Samples were spun twice at 800g, 5m at 4C and the aqueous phase removed. The rest of the protocol was performed as described in Skene et al., 2018 (3). For library preparation, the Rubicon Thruplex 12s DNA-seq kit was used following the manufacturer's protocol until the amplification step. For amplification, after the addition of indexes, 16-21 cycles of 98C, 20s; 67C, 10s were run. A 1.2x SPRI bead cleanup was performed (Agencourt Ampure XP). Libraries were sequenced on an Illumina MiSeq. The following antibody concentrations were used: 1:300 mouse anti-FLAG M2 (Sigma F1804); 1:200 rabbit anti-Mouse (Abcam ab46450); 1:400 Batch#6 proteinA-MNase (from Steven Henikoff).

RNA Sequencing Analysis

Reads were aligned with STAR (2.5.1b) (4). Indexes for STAR were generated with parameter --sjdbOverhang 49 using genome files for the dm3 reference genome. The STAR aligner was run with parameters --alignIntronMax 50000 --alignMatesGapMax 50000. Subread (v1.24.2) was used to count reads mapping to features (5). DESeq2 (v1.14.1) was used to identify differentially expressed genes using the lfcShrink function to shrink log-fold changes (6). Differentially expressed genes were defined as genes with an adjusted p-value less than 0.05 and a $\log_2$-fold change greater than 2. Normalized counts were generated using the counts function in DESeq2. For k-medoids clustering, normalized counts were first converted into the fraction of maximum WT counts and clustering was performed using the cluster package in R. Optimal cluster number was determined by minimizing the cluster silhouette. Heatmaps were generated using pheatmap (v1.0.10) in R. Gene Ontology analysis was performed using Bioconductor packages TopGO (v2.26.0) and GenomicFeatures (v1.26.4) using expressed genes as a background set with parameters: algorithm = 'elim' and statistic = 'fisher'. (7, 8). Expressed genes were defined as genes that remained after DESeq2 performed independent filtering to remove genes with low counts.

CUT&RUN Sequencing Analysis

Technical replicates were merged by concatenating fastq files. Reads were trimmed using bbmap (v37.50) with parameters ktrim=4 ref=adapters rcomp=t tpe=t tbo=t hdist=1 mink=11. Trimmed reads were aligned to the dm3 reference genome using Bowtie2 (v2.2.8) with parameters --local --very-sensitive-local --no-unal --no-mixed --no-discordant --phred33 -I 10 -X 700 (9). Reads with a quality score less than 5 were removed with samtools (v1.3.1) (10). PCR duplicates were marked with Picard (v2.2.4) and then removed with samtools. Bam files were converted to bed files with bedtools (v2.25.0) with parameter -bedpe and split into different fragment size categories using awk (11). Bedgraphs were generated with bedtools and then converted into bigwigs with ucsctools (v320) (12). Data was z-normalized using a custom R script. MACS

(v2016-02-15) was used to call peaks on individual replicates and merged files using a control genomic DNA file from sonicated genomic DNA using parameters -g 121400000 --nomodel --seed 123 (13). A final peak set was obtained by using peaks that were called in the merged file that overlapped with a peak called in at least one replicate. Heatmaps and average signal plots were generated from z-normalized data using the Bioconductor package Seqplots (v1.18.0). ChIPpeakAnno (v3.14.0) was used to calculate distance of peaks to their nearest gene (14, 15). Gene ontology analysis was performed as described for RNA-seq data, except that all genes were used as a background set. To identify clusters of EcR binding sites, the EcR peaks were resized to 5000bp, assigned to clusters, and the furthest start and end coordinate of the original peaks were used. To shuffle clusters, bedtools shuffle was used using –seed 100, including (-incl) peaks from WT FAIRE (2)

Motif Analysis

De novo motif analysis was performed using DREME (v4.12.0) using parameters -maxk 13 -t 18000 -e 0.05 (16). As background sequences, FAIRE peaks from -6hAPF or +6hAPF were used. To identify occurrences of the EcR motif in the genome, PWMs for the EcR and Usp motifs identified by a bacterial 1-hybrid were obtained from Fly Factor Survey (17). For the palindromic, Usp/EcR motif, the PWMs for EcR and Usp were concatenated together and the probabilities for the central, overlapping base were averaged. FIMO (v4.12.0) was run on the dm3 reference genome using parameters –max-stored-scores 10000000 --max-strand --no-qvalue --parse-genomic-coord --verbosity 4 --thresh 0.01 (18). Motif density plots were generated by counting the number of motifs around peak summits (10bp bins) and normalizing by the number of input peaks.

Drosophila culture and genetics

Flies were grown at 25C under standard culture conditions. Late wandering larvae were used as the –6hAPF timepoint. White prepupae were used as the 0h time point for staging +6hAPF animals. For 96hAEL, apple juice plates with embyos were cleared of any larvae and then four

hours later any animals that had hatched were transferred to vials. The following genotypes were used:

yw; vg-GAL4, UAS-FLP, UAS-GFP, Tub>>CD2>>GAL4 / CyO (19)

w^{1118}*; P{UAS-EcR-RNAi}104* (BDSC#9327)

yw; EcR^{GFSTF} (BDSC#59823)

w1118; Df(2R)BSC889/CyO (BDSC#32253)

UAS-dsGFP (gift of Brian McCabe)

usp3, w, P{neoFRT}19A/FM7c* (BDSC#64295)

P{Ubi-mRFP.nls}1, w, P{hsFLP}12 P{neoFRT}19A* (BDSC#31418)

w; UAS-EcR.B2.W650A (BDSC#9449)

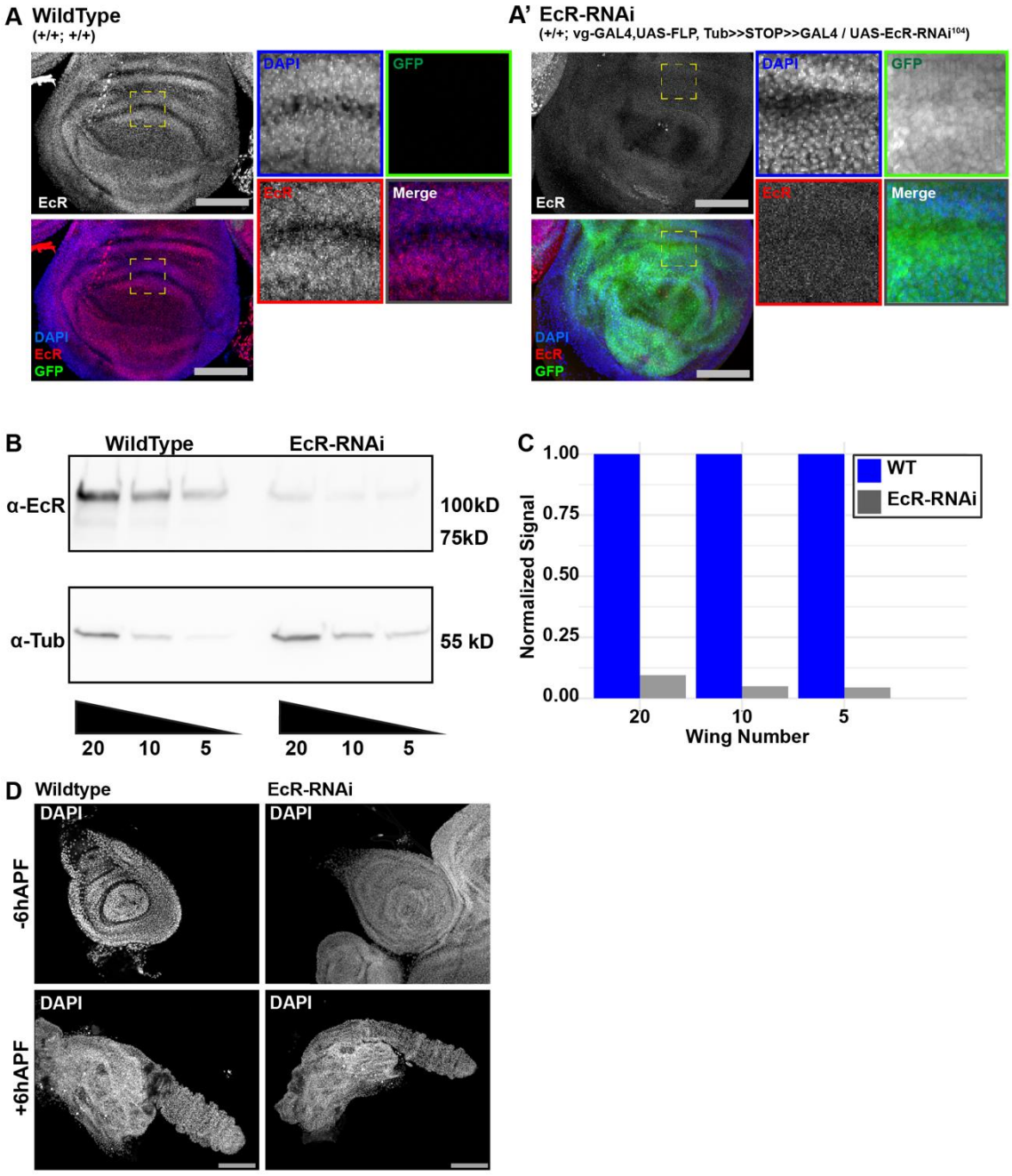

Fig. S1. EcR-RNAi knock down is effective and does not result in systemic developmental arrest

(A) WT and *vg-GAL4, UAS-FLP, Tub>>CD2>>GAL4, UAS-GFP; UAS-EcR-RNAi* (hereafter EcR-RNAi) wings at –6hAPF. Activity of *vg-GAL4* throughout the wing primordia causes flip-out of the STOP (CD2) cassette, resulting in persistent GAL4 expression throughout the wing. Location of insets is indicated by dashed boxes. (B) Western blots of EcR and alpha-tubulin levels in WT and EcR-RNAi wings from a serial dilution of wing tissue (wing number indicated below) . (C) Quantification of western blots normalized to alpha-tubulin expressed as the fraction

of WT signal. (D) Legs from WT and EcR-RNAi legs at –6hAPF and +6hAPF. Scale bars are 100μm.

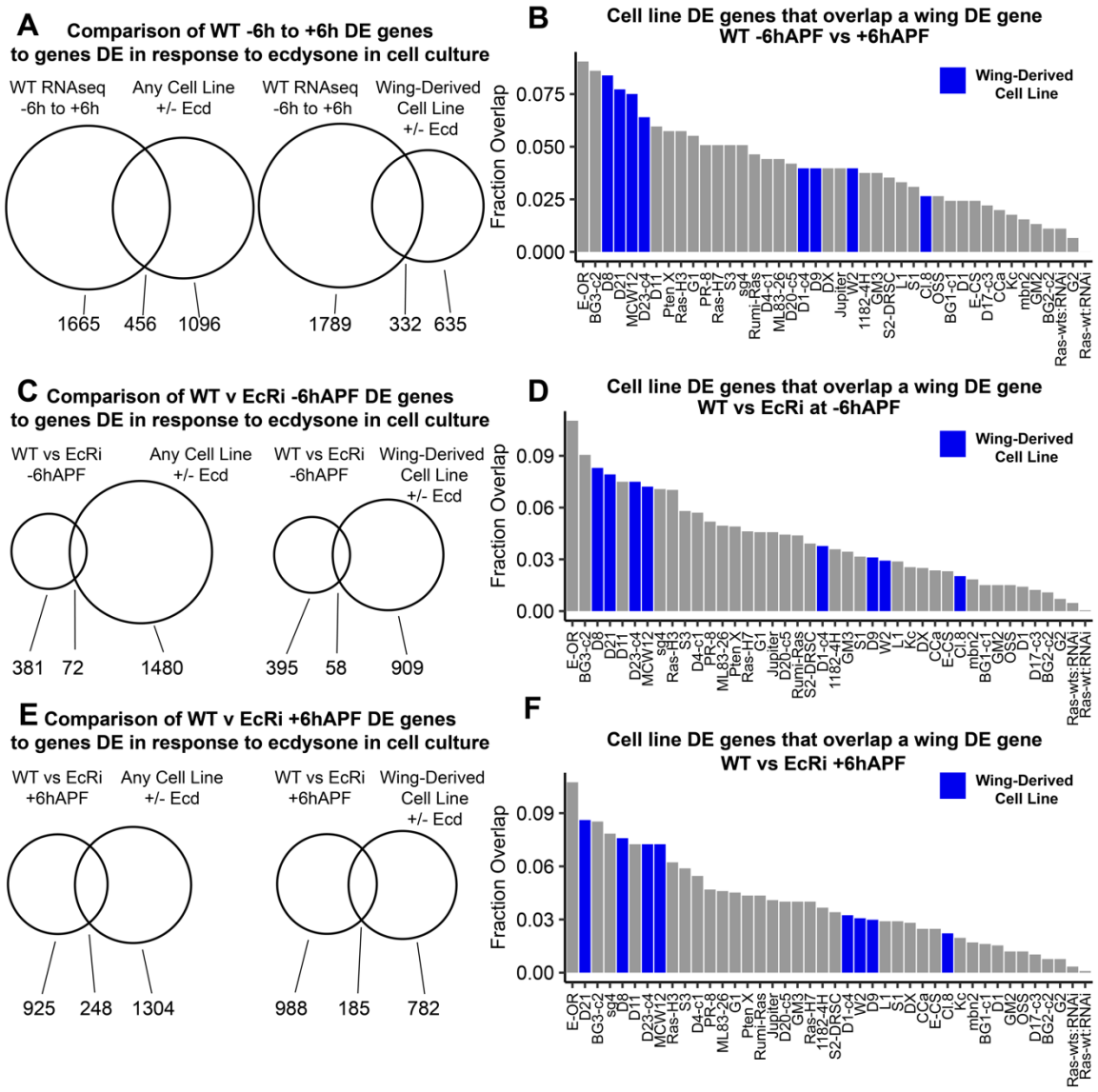

Figure S2: Comparison with Stoiber et al., 2016 (20)**.**
(A) Venn diagrams depicting the overlap between WT –6hAPF to +6hAPF differentially expressed (DE) genes and those that respond to ecdysone in any cell line (left) or in any wing-derived cell line (right). Wing-derived cell lines are highlighted in blue in the bar plots. (B) Bar plot of the fraction of DE genes in WT wings between –6hAPF and +6hAPF that overlap a gene differentially expressed in response to ecdysone in each indicated cell line. (C-D) Venn diagrams and bar plots as in A-B for –6hAPF WT vs EcR-RNAi (ECRi) DE genes (D-E) Venn diagrams and bar plots as in A-B for +6hAPF WT vs EcRi DE genes.

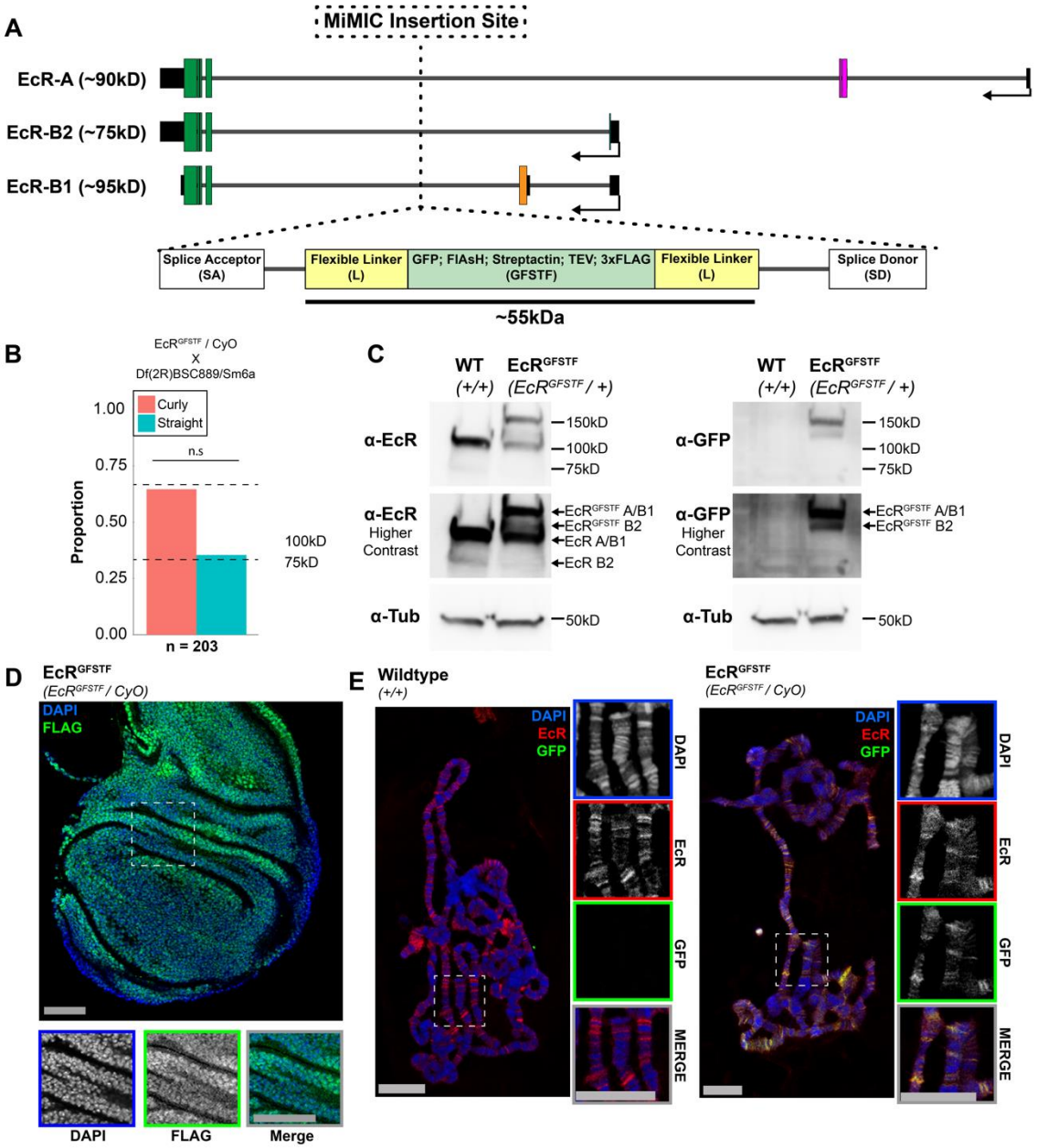

Fig. S3. The EcR^{GFSTF} tag does not impair EcR function

(A) Schematic of the *EcR*^{GFSTF} line generated by the *Drosophila* Gene Disruption Project (21–23). The line was generated through integration of a *Minos* transposon into a coding intron of the *EcR* locus. Subsequently, recombination-mediated cassette exchange was used to create an EcR protein trap containing the GFSTF tag (21, 22). The structure and size of the tag is indicated below the gene models. The insertion point is upstream of all exons shared between EcR isoforms and downstream of all isoform-specific exons. (B) Viability assay of *EcR*^{GFSTF} animals crossed to a deficiency spanning the EcR locus. Statistical significance was determined using a chi-squared test with an expected ratio of 1:2 homozygous to heterozygous animals. (C) Western blots of wings from *EcR*^{GFSTF} or *WT* animals stained for EcR or EcR^{GFSTF} (anti-GFP). EcR isoforms A/B1 and B2 are predicted to be ~150kD and ~125kD when the EcR^{GFSTF} tag is incorporated,

respectively. The western blot indicates both the 150kD and 125kD isoforms are trapped, and relative isoform abundance is maintained. (D) Immunostaining for EcR^{GFSTF} (anti-FLAG) shows nuclear localization in wings. Scale bars are 50µm (E) Polytene squashes from *WT* or EcR^{GFSTF} indicate EcR^{GFSTF} binds DNA. Scale bars are 25µm. Dashed boxes indicate the location of insets.

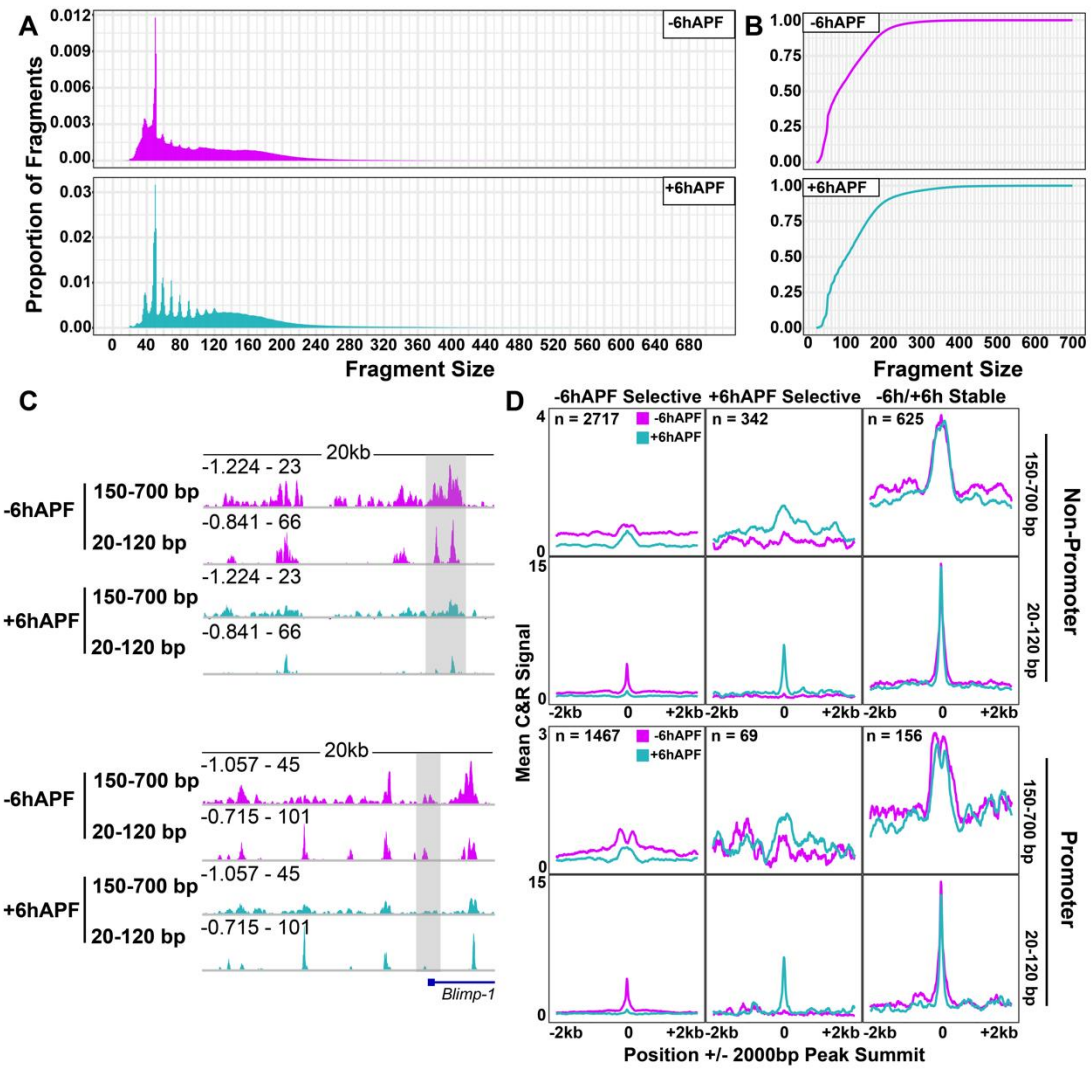

Fig. S4. EcR CUT&RUN exhibits similar properties to those that have been previously reported

(A) Histograms of fragment sizes from EcR CUT&RUN (C&R). (B) Cumulative distribution plot of fragment sizes. (C) Representative browser shots comparing EcR C&R signal from 20-120bp fragments and 150-700bp. (D) Average signal plots of EcR C&R signal split by overlap with annotated promoters and fragment size.

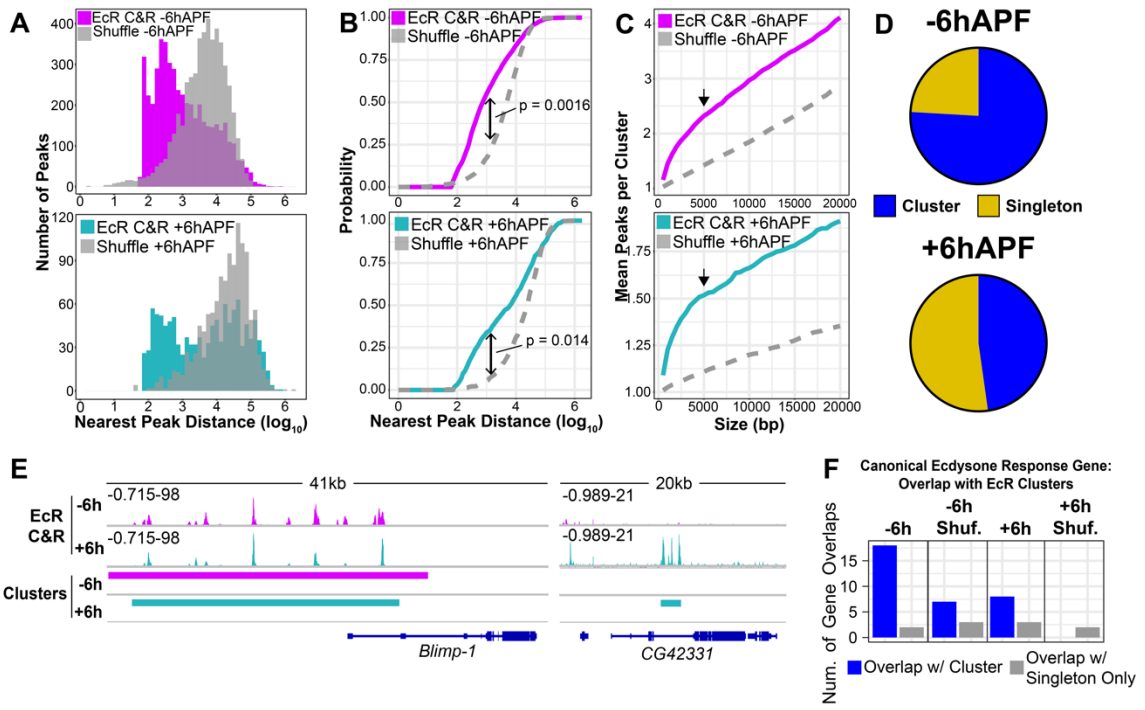

Fig. S5. EcR peaks are clustered genome-wide

(A) Histograms of distance of each EcR peak to its nearest neighbor compared to a peak set shuffled over FAIRE peaks. (B) Cumulative distribution plots of the distance of each EcR peak to its nearest neighbor compared to shuffled peaks. Distributions were compared with a KS-test. (C) The mean number of peaks that overlap at least one other peak using different sizes of EcR peak. Peaks within 5kb (arrow) of each other were merged into a single cluster for subsequent analyses. (D) Numbers of EcR peaks that fall into a cluster at –6hAPF and +6hAPF. (E) Examples of EcR clusters. (F) Numbers of canonical ecdysone-response genes that overlap an EcR cluster and those that only overlap an EcR singleton (ie. non-clustered peak) compared to clusters or singletons shuffled over open chromatin peaks. A list of canonical ecdysone response genes was generated by taking the union set of genes in gene ontology terms: Cellular response to ecdysone (GO:0071390); Steroid hormone mediated signaling pathway (GO:0043401) and appending all “Eip” (ecdysone induce protein) and “Imp” genes (40 total, see Table S3).

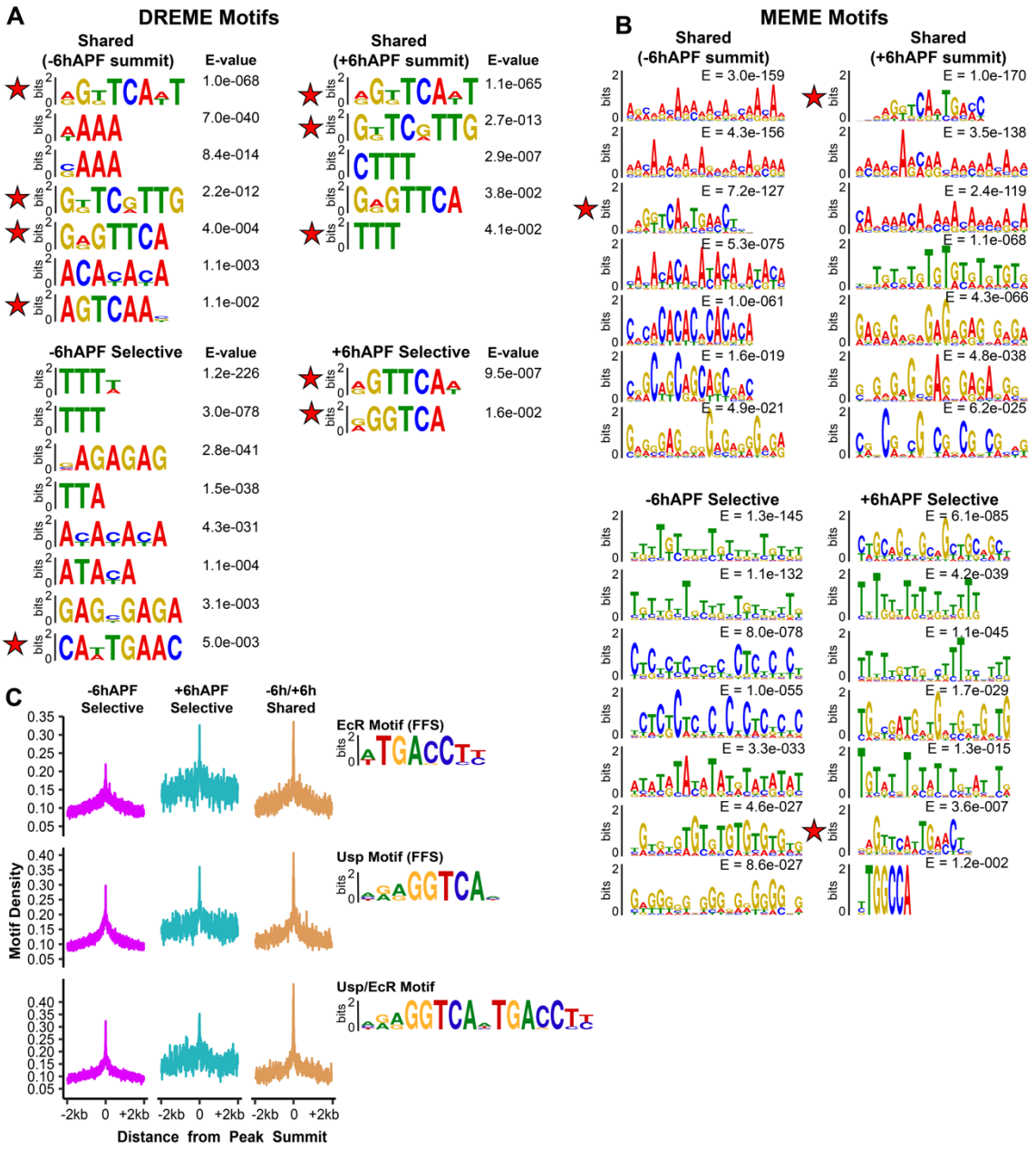

Figure S6. Motifs identified in EcR binding sites

(A) A full list of *de novo* motifs identified by DREME. (B) The top seven *de novo* motifs identified by MEME. For *de novo* motif identification, +/- 200bp from peak summit was used (see methods for details). Stars denote matches to the EcR motif or the EcR/Usp palindrome. (C) Motif density plots around the summits of EcR binding sites using motifs identified by bacterial 1-hybrid (17).The canonical motif was generated by combining the EcR and Usp PWMs together.

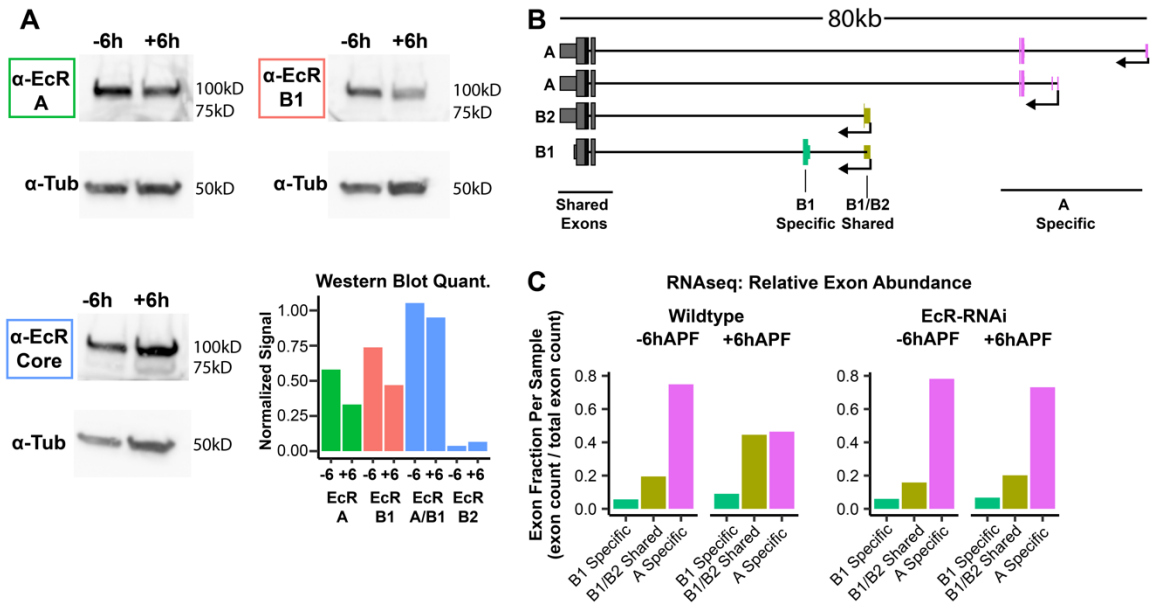

Figure S7: EcR isoforms levels over time

(A) Western blots depicting levels of EcR levels at –6hAPF and +6hAPF using isoform specific antibodies (EcR-A and EcR-B1) and an antibody that recognizes all EcR isoforms (EcR-core). Quantification of the core was performed by separately quantifying the top band, corresponding to EcR-A/B1, and the bottom band, corresponding to EcR-B2. The signal was normalized to tubulin. (B) Schematic of the EcR locus indicating exons shared between all isoforms (grey), exons specific to EcR-B1 (green), exons shared between EcR-B1 and EcR-B2 (yellow) and exons specific to EcR-A (pink). Note that EcR-A contains alternative 5'UTRs that do not affect the protein coding sequence. (C) Proportion of each exon type present at each time point. Exon counts were normalized to length.

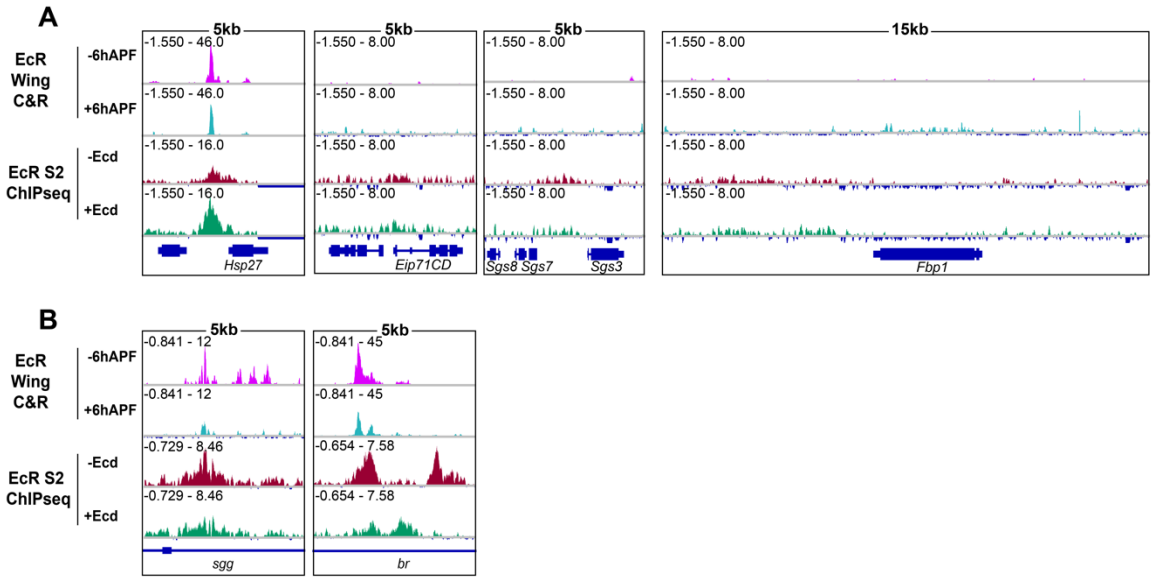

Fig. S8. EcR binding is absent in wings and S2 cells from many sites previously identified as functional EcR binding sites in other tissues

(A) Browser shots showing EcR C&R signal and S2 ChIPseq (24) at previously identified EcR binding sites. (B) Browser shots comparing precision of EcR binding between EcR and S2 cells.

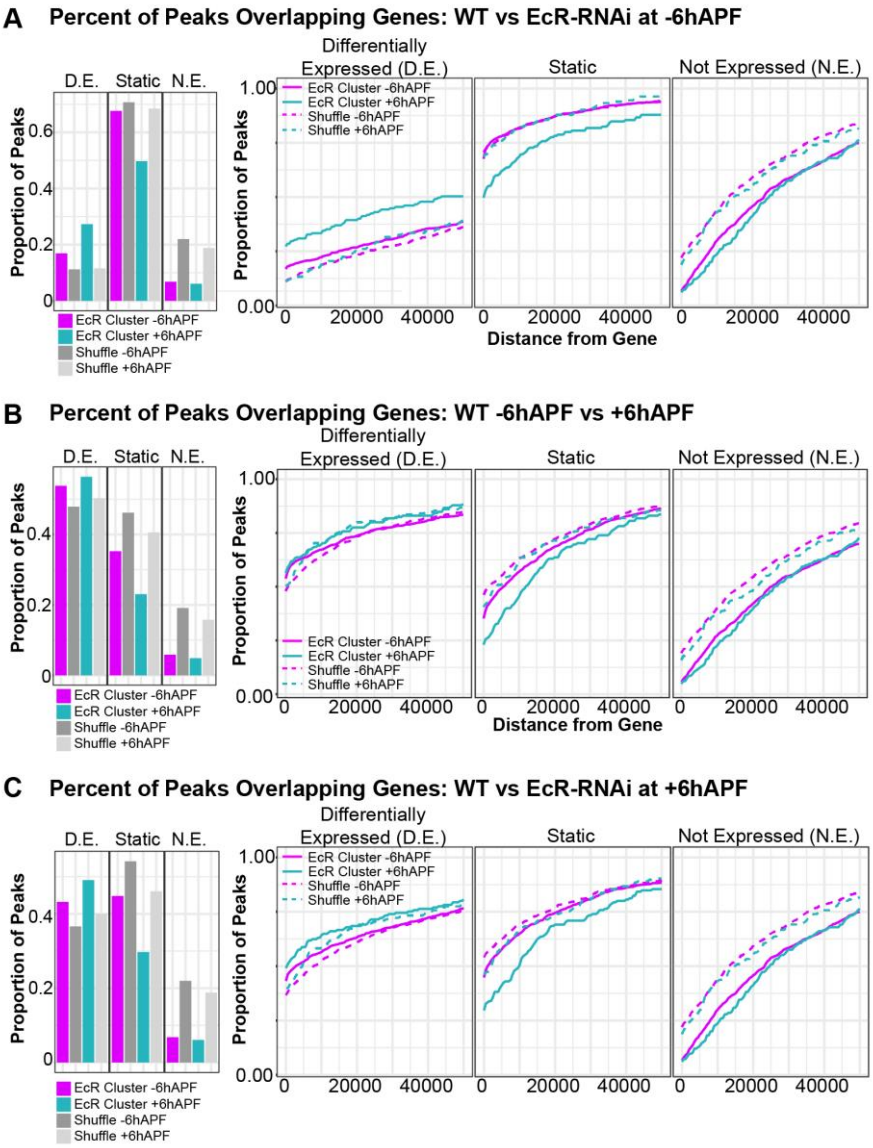

Fig. S9. EcR binding is enriched at genes that are affected by EcR knockdown

Percentage of EcR clusters that overlap (barplots, left), or fall within some distance of (cumulative distribution plots, right), a differentially expressed (D.E.), static, or not-expressed (N.E.) gene in RNAseq comparing (A) WT to EcR-RNAi wings at –6hAPF, (B) WT –6hAPF to +6hAPF, (C) WT to EcR-RNAi at +6hAPF. EcR peaks were compared to peaks randomly shuffled over FAIRE peaks. Differentially expressed genes were defined as genes with an adjusted p-value < 0.05. Not expressed genes were defined as genes that were filtered out by DESeq2 (padj = NA). Overlapping genes were defined as genes that overlapped a CUT&RUN peak by at least a single base pair. Note that separately examining up- and down-regulated genes in EcRi wings at either time point did not result in a statistically-significant correlation between EcR binding and differential gene expression.

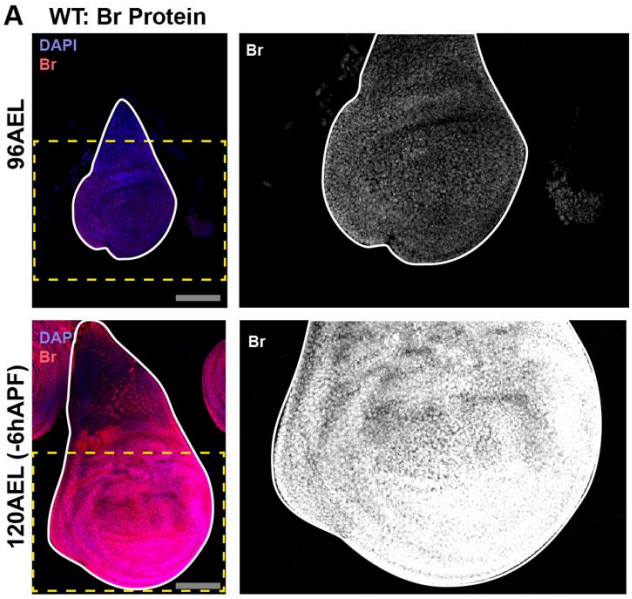

Fig. S10. Broad protein levels increase with time.
(A) Changes in Br protein (red) levels over time in WT wings between 96hrs after egg laying (96AEL) and 120AEL (-6hAPF). Scale bars are 100um. DAPI was used to stain nuclei.

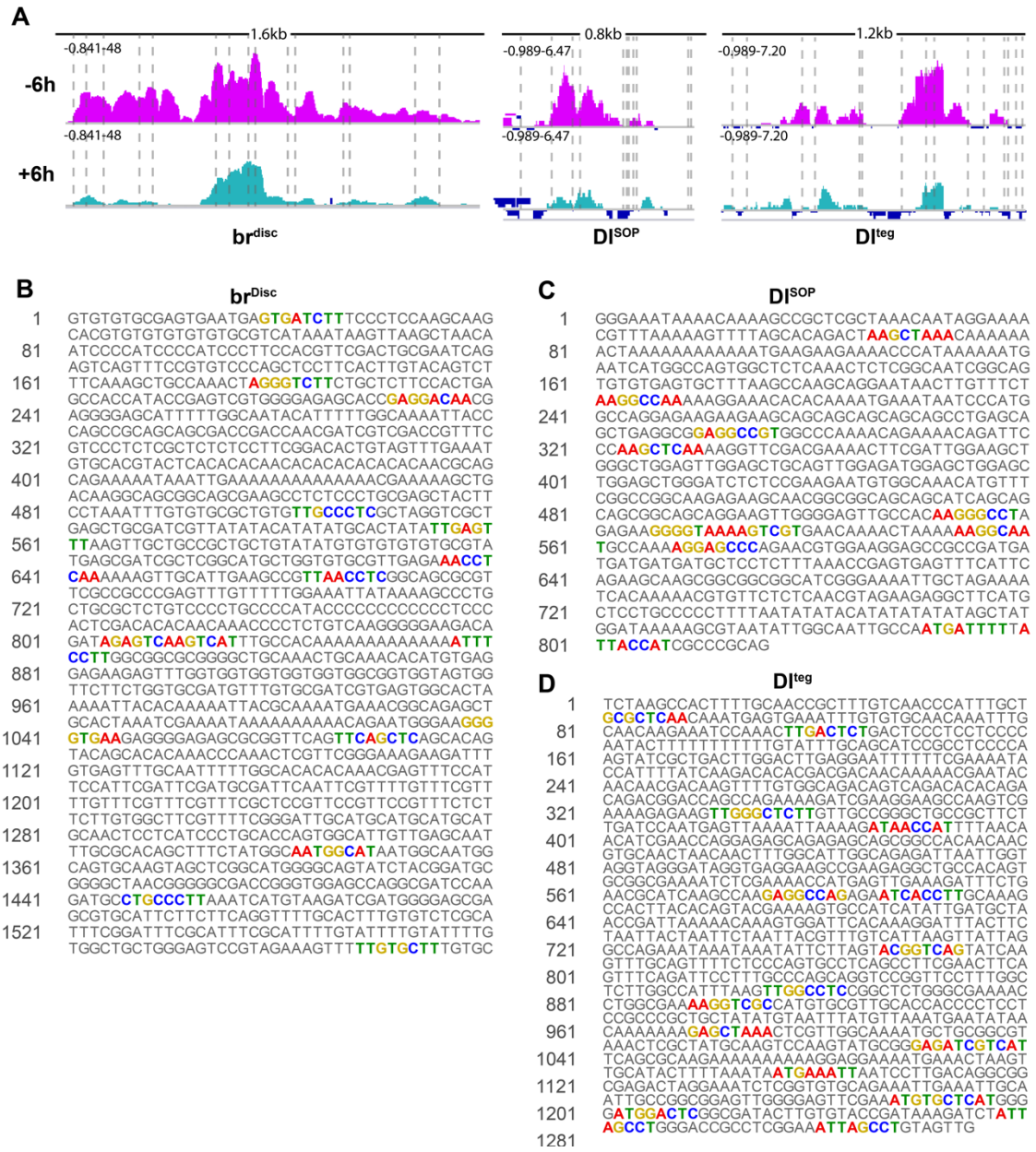

Fig. S11. Motif content inside br and Dl enhancers.

(A) Browser shots of the three enhancers examined in this study. The width of each browser corresponds to the enhancer boundaries. The locations of EcR motifs are indicated with dashed lines. (B-D) Enhancer sequences for *br*^{disc}, *Dl*^{SOP}, and *Dl*^{teg}. EcR motifs are indicated by coloring the bases. The EcR motif from Fly Factor Survey (17) was used.

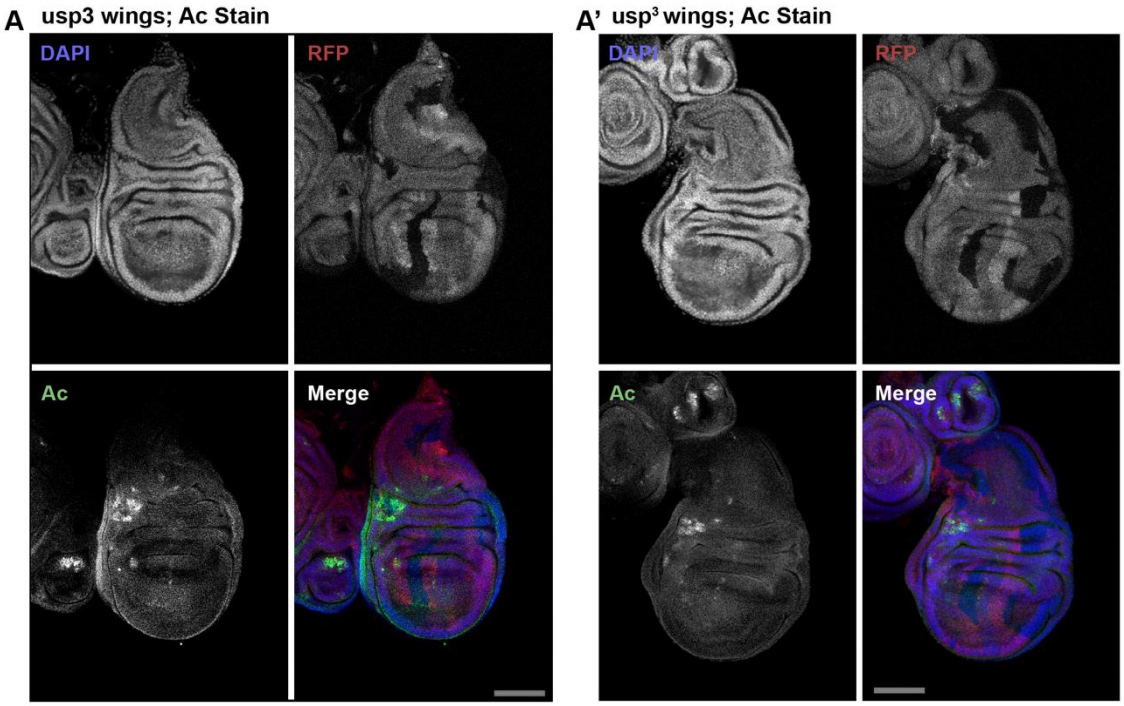

Fig. S12: usp^3 clones to not result in cell fate changes
(A) –6hAPF wings showing *usp^3* mitotic clones stained for Ac. Clones are marked by the absence of RFP. Scale bars are 100um. DAPI was used to stain nuclei.

Table S1: Gene Ontology Terms for EcR Clusters at –6hAPF (top five)

Behavior	Cluster	GO.ID	Term	p-value (-log10)
ECRi –6hAPF > WT –6hAPF	1	GO:0015833	peptide transport	2.508638306
ECRi –6hAPF > WT –6hAPF	1	GO:0035848	oviduct morphogenesis	2.356547324
ECRi –6hAPF > WT –6hAPF	1	GO:0010898	positive regulation of triglyceride catabolic process	2.356547324
ECRi –6hAPF > WT –6hAPF	1	GO:0010716	negative regulation of extracellular matrix disassembly	2.356547324
ECRi –6hAPF > WT –6hAPF	1	GO:0048621	post-embryonic digestive tract morphogenesis	2.356547324
ECRi –6hAPF > WT –6hAPF	2	GO:0008063	Toll signaling pathway	4.886056648
ECRi –6hAPF > WT –6hAPF	2	GO:0040003	chitin-based cuticle development	3.744727495
ECRi –6hAPF > WT –6hAPF	2	GO:0035074	pupation	3.148741651
ECRi –6hAPF > WT –6hAPF	2	GO:0006965	positive regulation of biosynthetic process of antibacterial peptides active against Gram-positive bacteria	2.928117993
ECRi –6hAPF > WT –6hAPF	2	GO:0016045	detection of bacterium	2.928117993
ECRi –6hAPF > WT –6hAPF	3	GO:0002028	regulation of sodium ion transport	3.443697499
ECRi –6hAPF > WT –6hAPF	3	GO:0045479	vesicle targeting to fusome	2.301899454
ECRi –6hAPF > WT –6hAPF	3	GO:0042554	superoxide anion generation	2.301899454
ECRi –6hAPF > WT –6hAPF	3	GO:0070731	cGMP transport	2.301899454
ECRi –6hAPF > WT –6hAPF	3	GO:0051597	response to methylmercury	2.301899454
ECRi –6hAPF > WT –6hAPF	4	GO:0040003	chitin-based cuticle development	18.95860731
ECRi –6hAPF > WT –6hAPF	4	GO:0003383	apical constriction	1.455931956
ECRi –6hAPF > WT –6hAPF	4	GO:0008362	chitin-based embryonic cuticle biosynthetic process	1.387216143
ECRi –6hAPF > WT –6hAPF	4	GO:0070252	actin-mediated cell contraction	1.387216143
ECRi –6hAPF > WT –6hAPF	4	GO:0042335	cuticle development	1.356547324
ECRi –6hAPF > WT –6hAPF	5	GO:0031427	response to methotrexate	3.958607315
ECRi –6hAPF > WT –6hAPF	5	GO:0007218	neuropeptide signaling pathway	3.244125144
ECRi –6hAPF > WT –6hAPF	5	GO:0006094	gluconeogenesis	2.36552273
ECRi –6hAPF > WT –6hAPF	5	GO:0009408	response to heat	2.191789027
ECRi –6hAPF > WT –6hAPF	5	GO:0035079	polytene chromosome puffing	1.998699067
WT –6hAPF > ECRi –6hAPF	1	GO:0071390	cellular response to ecdysone	3.602059991
WT –6hAPF > ECRi –6hAPF	1	GO:0009597	detection of virus	2.872895202
WT –6hAPF > ECRi –6hAPF	1	GO:0006833	water transport	2.571865206
WT –6hAPF > ECRi –6hAPF	1	GO:0071329	cellular response to sucrose stimulus	2.395773947
WT –6hAPF > ECRi –6hAPF	1	GO:0007610	behavior	2.381951903
WT –6hAPF > ECRi –6hAPF	2	GO:0043401	steroid hormone mediated signaling pathway	3.214670165
WT –6hAPF > ECRi –6hAPF	2	GO:0045200	establishment of neuroblast polarity	2.302770657
WT –6hAPF > ECRi –6hAPF	2	GO:0090163	establishment of epithelial cell planar polarity	2.302770657
WT –6hAPF > ECRi –6hAPF	2	GO:0072697	protein localization to cell cortex	2.302770657
WT –6hAPF > ECRi –6hAPF	2	GO:0016336	establishment or maintenance of polarity of larval imaginal disc epithelium	2.206209615
WT –6hAPF > ECRi –6hAPF	3	GO:0035320	imaginal disc-derived wing hair site selection	2.187086643

WT –6hAPF > ECRi –6hAPF	3	GO:0071632	optomotor response	2.187086643
WT –6hAPF > ECRi –6hAPF	3	GO:0019752	carboxylic acid metabolic process	2.173925197
WT –6hAPF > ECRi –6hAPF	3	GO:0009408	response to heat	2.086186148
WT –6hAPF > ECRi –6hAPF	3	GO:0001676	long-chain fatty acid metabolic process	1.943095149

Table S2: Gene Ontology Terms for EcR Clusters at +6hAPF (top five)

Behavior	Cluster	GO.ID	Term	p-value (-log10)
ECRi +6hAPF > WT +6hAPF	1	GO:0006030	chitin metabolic process	2.853871964
ECRi +6hAPF > WT +6hAPF	1	GO:0090100	positive regulation of transmembrane receptor protein serine/threonine kinase signaling pathway	2.13076828
ECRi +6hAPF > WT +6hAPF	1	GO:0006784	heme a biosynthetic process	1.991399828
ECRi +6hAPF > WT +6hAPF	1	GO:0046160	heme a metabolic process	1.991399828
ECRi +6hAPF > WT +6hAPF	1	GO:0001837	epithelial to mesenchymal transition	1.991399828
ECRi +6hAPF > WT +6hAPF	2	GO:0007052	mitotic spindle organization	11.32790214
ECRi +6hAPF > WT +6hAPF	2	GO:0009267	cellular response to starvation	10.85387196
ECRi +6hAPF > WT +6hAPF	2	GO:0006364	rRNA processing	8.721246399
ECRi +6hAPF > WT +6hAPF	2	GO:0022008	neurogenesis	6.958607315
ECRi +6hAPF > WT +6hAPF	2	GO:0042254	ribosome biogenesis	6.522878745
ECRi +6hAPF > WT +6hAPF	3	GO:0002028	regulation of sodium ion transport	3.408935393
ECRi +6hAPF > WT +6hAPF	3	GO:0055072	iron ion homeostasis	2.747146969
ECRi +6hAPF > WT +6hAPF	3	GO:0034605	cellular response to heat	2.385102784
ECRi +6hAPF > WT +6hAPF	3	GO:0042335	cuticle development	2.12090412
ECRi +6hAPF > WT +6hAPF	3	GO:0045479	vesicle targeting to fusome	2.086716098
ECRi +6hAPF > WT +6hAPF	4	GO:0040003	chitin-based cuticle development	17.04095861
ECRi +6hAPF > WT +6hAPF	4	GO:0048082	regulation of adult chitin-containing cuticle pigmentation	2.920818754
ECRi +6hAPF > WT +6hAPF	4	GO:0045187	regulation of circadian sleep/wake cycle, sleep	2.537602002
ECRi +6hAPF > WT +6hAPF	4	GO:0048066	developmental pigmentation	2.283996656
ECRi +6hAPF > WT +6hAPF	4	GO:0001692	histamine metabolic process	2.229147988
WT +6hAPF > ECRi +6hAPF	1	GO:0045214	sarcomere organization	3.366531544
WT +6hAPF > ECRi +6hAPF	1	GO:0007525	somatic muscle development	2.950781977
WT +6hAPF > ECRi +6hAPF	1	GO:0060402	calcium ion transport into cytosol	2.850780887
WT +6hAPF > ECRi +6hAPF	1	GO:0006869	lipid transport	2.705533774
WT +6hAPF > ECRi +6hAPF	1	GO:0010888	negative regulation of lipid storage	2.554395797
WT +6hAPF > ECRi +6hAPF	2	GO:0055085	transmembrane transport	3.251811973
WT +6hAPF > ECRi +6hAPF	2	GO:0010025	wax biosynthetic process	2.954677021
WT +6hAPF > ECRi +6hAPF	2	GO:0007320	insemination	2.657577319
WT +6hAPF > ECRi +6hAPF	2	GO:0006508	proteolysis	2.345823458
WT +6hAPF > ECRi +6hAPF	2	GO:0042752	regulation of circadian rhythm	2.301899454
WT +6hAPF > ECRi +6hAPF	3	GO:0008299	isoprenoid biosynthetic process	7.113509275
WT +6hAPF > ECRi +6hAPF	3	GO:0051923	sulfation	3.698970004
WT +6hAPF > ECRi +6hAPF	3	GO:0006805	xenobiotic metabolic process	3.408935393
WT +6hAPF > ECRi +6hAPF	3	GO:0003383	apical constriction	3.107905397
WT +6hAPF > ECRi +6hAPF	3	GO:0006030	chitin metabolic process	2.728158393
WT +6hAPF > ECRi +6hAPF	4	GO:0071329	cellular response to sucrose stimulus	2.431798276
WT +6hAPF > ECRi +6hAPF	4	GO:0050709	negative regulation of protein secretion	2.251811973

WT +6hAPF > ECRi +6hAPF	4	GO:0001676	long-chain fatty acid metabolic process	1.954677021
WT +6hAPF > ECRi +6hAPF	4	GO:0009651	response to salt stress	1.829738285
WT +6hAPF > ECRi +6hAPF	4	GO:0006970	response to osmotic stress	1.655607726

Table S3: Canonical Ecdysone Response Genes

Category	Gene ID
GO:0043401 (Steroid Hormone Mediated Signaling Pathway)	dsf
GO:0043401 (Steroid Hormone Mediated Signaling Pathway)	eg
GO:0043401 (Steroid Hormone Mediated Signaling Pathway)	Eip75B
GO:0043401 (Steroid Hormone Mediated Signaling Pathway)	Eip78C
GO:0043401 (Steroid Hormone Mediated Signaling Pathway)	ERR
GO:0043401 (Steroid Hormone Mediated Signaling Pathway)	ftz-f1
GO:0043401 (Steroid Hormone Mediated Signaling Pathway)	Hnf4
GO:0043401 (Steroid Hormone Mediated Signaling Pathway)	Hr38
GO:0043401 (Steroid Hormone Mediated Signaling Pathway)	Hr39
GO:0043401 (Steroid Hormone Mediated Signaling Pathway)	Hr3
GO:0043401 (Steroid Hormone Mediated Signaling Pathway)	Hr51
GO:0043401 (Steroid Hormone Mediated Signaling Pathway)	Hr78
GO:0043401 (Steroid Hormone Mediated Signaling Pathway)	Hr83
GO:0043401 (Steroid Hormone Mediated Signaling Pathway)	Hr96
GO:0043401 (Steroid Hormone Mediated Signaling Pathway)	knrl
GO:0043401 (Steroid Hormone Mediated Signaling Pathway)	svp
GO:0043401 (Steroid Hormone Mediated Signaling Pathway)	tll
GO:0043401 (Steroid Hormone Mediated Signaling Pathway)	usp
GO:0071390 (Cellular Response to Ecdysone)	Blimp-1
GO:0071390 (Cellular Response to Ecdysone)	br
GO:0071390 (Cellular Response to Ecdysone)	Eip93F
GO:0071390 (Cellular Response to Ecdysone)	let-7-C
GO:0071390 (Cellular Response to Ecdysone)	Lpt
GO:0071390 (Cellular Response to Ecdysone)	MED27
GO:0071390 (Cellular Response to Ecdysone)	Sgs3
GO:0071390 (Cellular Response to Ecdysone)	usp
GO:0071390 (Cellular Response to Ecdysone)	Utx
Other Ecdysone Response Genes	Eip55E
Other Ecdysone Response Genes	Eip63E
Other Ecdysone Response Genes	Eip63F-1
Other Ecdysone Response Genes	Eip63F-2
Other Ecdysone Response Genes	Eip71CD
Other Ecdysone Response Genes	Eip74EF
Other Ecdysone Response Genes	Imp
Other Ecdysone Response Genes	ImpE1
Other Ecdysone Response Genes	ImpE2
Other Ecdysone Response Genes	ImpE3

Other Ecdysone Response Genes	ImpL1
Other Ecdysone Response Genes	ImpL2
Other Ecdysone Response Genes	ImpL3

Table S4: Gene Ontology Terms for EcR Binding Sites (top five)

Overlap Type	GO.ID	Term	p-value (-log10)
+6hAPF Unique	GO:0007476	imaginal disc-derived wing morphogenesis	4.040958608
+6hAPF Unique	GO:0002009	morphogenesis of an epithelium	3.420216403
+6hAPF Unique	GO:0035152	regulation of tube architecture, open tracheal system	3.366531544
+6hAPF Unique	GO:0018107	peptidyl-threonine phosphorylation	3.236572006
+6hAPF Unique	GO:0007370	ventral furrow formation	3.207608311
-6h/+6h Stable	GO:0007476	imaginal disc-derived wing morphogenesis	8.142667504
-6h/+6h Stable	GO:0048190	wing disc dorsal/ventral pattern formation	6.259637311
-6h/+6h Stable	GO:0007156	homophilic cell adhesion via plasma membrane adhesion molecules	5.15490196
-6h/+6h Stable	GO:0007411	axon guidance	4.853871964
-6h/+6h Stable	GO:0016318	ommatidial rotation	4.769551079
-6hAPF Unique	GO:0000122	negative regulation of transcription from RNA polymerase II promoter	20.92081875
-6hAPF Unique	GO:0007476	imaginal disc-derived wing morphogenesis	20.76955108
-6hAPF Unique	GO:0007411	axon guidance	15.38721614
-6hAPF Unique	GO:0045944	positive regulation of transcription from RNA polymerase II promoter	14.88605665
-6hAPF Unique	GO:0035277	spiracle morphogenesis, open tracheal system	12.18045606

References

1. Jiang L, Pearson JC, Crews ST (2010) Diverse modes of Drosophila tracheal fusion cell transcriptional regulation. *Mech Dev* 127(5–6):265–280.

2. McKay DJ, Lieb JD (2013) A common set of DNA regulatory elements shapes Drosophila appendages. *Dev Cell* 27(3):306–318.

3. Skene PJ, Henikoff JG, Henikoff S (2018) Targeted in situ genome-wide profiling with high efficiency for low cell numbers. *Nat Protoc* 13(5):1006–1019.

4. Dobin A, et al. (2013) STAR: ultrafast universal RNA-seq aligner. *Bioinformatics* 29(1):15–21.

5. Liao Y, Smyth GK, Shi W (2013) The Subread aligner: fast, accurate and scalable read mapping by seed-and-vote. *Nucleic Acids Res* 41(10):e108.

6. Love MI, Huber W, Anders S (2014) Moderated estimation of fold change and dispersion for RNA-seq data with DESeq2. *Genome Biology* 15:550.

7. Rahnenfuhrer AAJ (2018) topGO. *topGO: Enrichment Analysis for Gene Ontology*. Available at: http://bioconductor.org/packages/topGO/ [Accessed November 26, 2018].

8. Lawrence M, et al. (2013) Software for computing and annotating genomic ranges. *PLoS Comput Biol* 9(8):e1003118.

9. Langmead B, Salzberg SL (2012) Fast gapped-read alignment with Bowtie 2. *Nat Methods* 9(4):357–359.

10. Li H, et al. (2009) The Sequence Alignment/Map format and SAMtools. *Bioinformatics* 25(16):2078–2079.

11. Quinlan AR, Hall IM (2010) BEDTools: a flexible suite of utilities for comparing genomic features. *Bioinformatics* 26(6):841–842.

12. Kent WJ, Zweig AS, Barber G, Hinrichs AS, Karolchik D (2010) BigWig and BigBed: enabling browsing of large distributed datasets. *Bioinformatics* 26(17):2204–2207.

13. Zhang Y, et al. (2008) Model-based Analysis of ChIP-Seq (MACS). *Genome Biology* 9:R137.

14. Stempor P, Ahringer J (2016) SeqPlots - Interactive software for exploratory data analyses, pattern discovery and visualization in genomics. *Wellcome Open Res* 1:14.

15. Zhu LJ, et al. (2010) ChIPpeakAnno: a Bioconductor package to annotate ChIP-seq and ChIP-chip data. *BMC Bioinformatics* 11:237.

16. Bailey TL (2011) DREME: motif discovery in transcription factor ChIP-seq data. *Bioinformatics* 27(12):1653–1659.

17. Zhu LJ, et al. (2011) FlyFactorSurvey: a database of Drosophila transcription factor binding specificities determined using the bacterial one-hybrid system. *Nucleic Acids Res* 39(Database issue):D111-117.

18. Grant CE, Bailey TL, Noble WS (2011) FIMO: scanning for occurrences of a given motif. *Bioinformatics* 27(7):1017–1018.

19. Crickmore MA, Mann RS (2006) Hox control of organ size by regulation of morphogen production and mobility. *Science* 313(5783):63–68.

20. Stoiber M, Celniker S, Cherbas L, Brown B, Cherbas P (2016) Diverse Hormone Response Networks in 41 Independent Drosophila Cell Lines. *G3* 6(3):683–694.

21. Nagarkar-Jaiswal S, et al. (2015) A library of MiMICs allows tagging of genes and reversible, spatial and temporal knockdown of proteins in Drosophila. *eLife* 4:e05338.

22. Nagarkar-Jaiswal S, et al. (2015) A genetic toolkit for tagging intronic MiMIC containing genes. *eLife* 4:e08469.

23. Venken KJT, et al. (2011) MiMIC: a highly versatile transposon insertion resource for engineering Drosophila melanogaster genes. *Nat Methods* 8(9):737–743.

24. Shlyueva D, et al. (2014) Hormone-responsive enhancer-activity maps reveal predictive motifs, indirect repression, and targeting of closed chromatin. *Mol Cell* 54(1):180–192.